Available online at www.sciencedirect.com
SCIENCE DIRECT®
Applied Mathematical Modelling 28 (2004) 775–794
APPLIED MATHEMATICAL MODELLING
www.elsevier.com/locate/apm

Transient modelling of flow distribution in automotive catalytic converters

D.N. Tsinoglou [a], G.C. Koltsakis [a,*], D.K. Missirlis [b], K.J. Yakinthos [b]

[a] *Laboratory of Applied Thermodynamics, Department of Mechanical Engineering, Aristotle University Thessaloniki, Thessaloniki 54124, Greece*

[b] *Laboratory of Fluid Mechanics and Turbomachinery, Aristotle University Thessaloniki, Thessaloniki 54124, Greece*

Received 6 August 2002; received in revised form 9 December 2003; accepted 16 December 2003
Available online 3 March 2004

Abstract

The transient catalytic converter performance is governed by complex interactions between exhaust gas flow and the monolithic structure of the catalytic converter. Therefore, during typical operating conditions of interest, one has to take into account the effect of the inlet diffuser on the flow field at the entrance. computational fluid dynamics (CFD) is a powerful tool for calculating the flow field inside the catalytic converter. Radial velocity profiles, obtained by a commercial CFD code, present very good agreement with respective experimental results published in the literature. However the applicability of CFD for transient simulations is limited by the high CPU demands.

The present study proposes an alternative computational method for the prediction of transient flow fields in axi-symmetric converters time-efficiently. The method is based on the use of equivalent flow resistances to simulate the flow paths in the inlet and outlet catalyst sections. The proposed flow resistance modelling (FRM) method is validated against the results of CFD predictions over a wide range of operating conditions. Apart from the apparent CPU advantages, the proposed methodology can be readily coupled with already available transient models for the chemical reactions in the catalyst. A transient model for heat transfer inside the monolith is presented. An example of coupling between FRM and transient heat transfer inside the converter is included. This example illustrates the effect of flow distribution in the thermal response of a catalytic converter, during the critical phase of catalytic converter warm-up.

Keywords: CFD; Catalytic converter; Flow distribution; Heat transfer

* Corresponding author. Tel.: +30-2310-995870; fax: +30-2310-996019.
E-mail address: greg@antiopi.meng.auth.gr (G.C. Koltsakis).

0307-904X/$ - see front matter © 2004 Elsevier Inc. All rights reserved.
doi:10.1016/j.apm.2003.12.006

Nomenclature

Variables

A	surface, m^2
C_p	specific heat capacity, J/kg K
d	diameter, m
h	convective heat transfer coefficient, W/m^2 K
k	turbulence kinetic energy, m^2/s^2
L	length, m
$\dot{m}$	mass flow rate, kg/s
Nu	Nusselt number, $Nu = \frac{h \cdot d_h}{\lambda_g}$
$\dot{q}$	heat transfer volumetric rate, W/m^3
r	radius, m
S	monolith specific surface area, m^2/m^3
t	time, s
T	temperature, K
Tu	turbulence level
x	axial distance from monolith entrance, m
x^*	dimensionless axial distance, $x^* = \frac{x}{d_h \cdot Re \cdot Pr}$
u	gas velocity, m/s
vfr	substrate void fraction

Greek letters

γ	flow uniformity index
ε	turbulence dissipation rate (CFD turbulence modelling), m^2/s^3 emissivity factor (transient heat transfer model)
μ	dynamic viscosity, kg/ms
ρ	density, kg/m^3
ζ	empirical factor for diffuser pressure loss
λ	thermal conductivity, W/mK
ξ	dimensionless length, $\xi = \frac{Nu \lambda_g S_i A_i \varepsilon_i}{d_{h,i} \dot{m}_i C_{p,g}} x$
σ	Stefan Boltzmann constant 5.67×10^8 W/m^2 K^4
ω	flow non-uniformity index

Subscripts

conv	convection
g	exhaust gas
h	hydraulic
i	radial node index
j	monolith index
k	axial node index
m	mass

out	outer
ref	reference
s	solid

1. Introduction

The monolithic catalytic converter remains the main pollution control device for modern automobiles towards reaching the ever-increasing legislative demands for low emission standards. The catalytic converter (Fig. 1) is expected to attain conversion efficiencies of the order of 95% or above for the main exhaust gas pollutants, namely CO, hydrocarbons and NO_x. The conversion efficiency is a function of numerous design and operating parameters of the complete system, comprising the engine, the exhaust line and the catalytic converter [1]. The design optimization task is especially demanding due to the highly unsteady conditions in the engine exhaust regarding temperature, flow rate and exhaust composition.

From the fluid dynamics point of view, the distribution of flow at the entrance area of the monolith is of special interest. This subject has attracted much research effort, including both experimental and modelling studies. It is generally claimed that a uniform flow distribution at the inlet monolith face is favorable for both the conversion efficiency as well as the durability of the catalytic converter [2]. Therefore, the main problem is to optimize the inlet pipe and diffuser geometry in order to minimize the flow maldistributions at catalyst inlet.

Experimental techniques have been employed to visualize the internal flow structure of a prototype monolith converter [3], concluding that the flow uniformity is a function of the inlet flow Reynolds number. Since then, computational methods relying mostly on computational fluid dynamics (CFD) software have been widely used to provide more detailed information on the flow field as function of various design and operating parameters. 3-D flow field simulations at steady-state conditions have been presented, including validation of the results with measurements [4]. The effect of inlet geometry on flow distribution has been studied by CFD and a flow uniformity index has been defined as a criterion to quantify the results [5]. More recent studies [6] have employed a comprehensive CFD-based modelling approach to predict the steady-state performance of the catalytic converter, including the effects of heat and mass transfer in the monolith, oxidation reactions, heat generation and ambient heat losses.

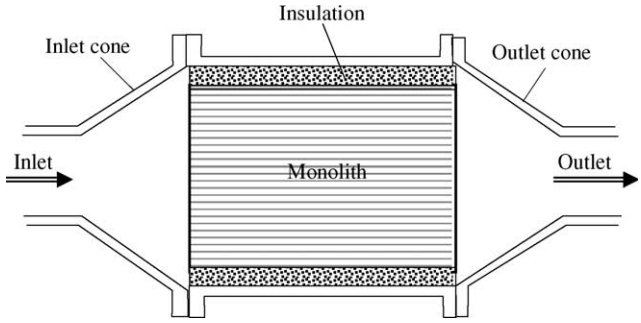

Fig. 1. Schematic of the catalytic converter considered in the present study. Dimensions are given in Table 1.

From the engineering point of view, it is of special interest to quantify the effect of flow distribution on the conversion efficiency of the catalytic converter under transient conditions resembling real-world operation. This can be done by coupling the results of the CFD simulations with mathematical models for the transport and chemical phenomena in the monolith channels. According to this approach, a simplified 2-D axi-symmetric model has been previously employed in order to reach reasonable computational times (less than one day) [7].

3-D simulations of complete systems including multiple catalyst monoliths placed along the exhaust line have also been presented [8]. The authors reported that a typical transient simulation with 1000 time steps required approximately 526.4 CPU hours, which is rather prohibitive for efficient optimization work. The problem of excessive CPU demands for transient CFD calculations has been addressed [9], the authors concluding that transient CFD analysis can be very helpful in the design of close-coupled catalyst designs, which become increasingly popular, even if one should cope with 1–2 orders of magnitude larger computational resources compared to steady-state simulations.

The aim of the present study is to propose an alternative computational method for the prediction of transient flow fields in axi-symmetric converters time-efficiently. The method is based on the use of equivalent flow resistances to simulate the flow paths in the inlet and outlet catalyst sections. The method is validated against the results of CFD predictions over a wide range of operating conditions. The CFD results are also validated against literature experimental results at selected operating conditions. Apart from the apparent CPU advantages, the methodology for flow distribution calculation can be readily coupled with already available transient models for the chemical reactions in the catalyst. The modelling approach will be illustrated by an example of catalyst predictions of the transient flow and temperature fields in a catalyst during engine warm-up.

2. CFD modelling

In this section, computational fluid dynamics is applied to calculate the pressure distribution and velocity field in the inlet and outlet cone. Fig. 1 shows the arrangement of the catalytic converter considered in the present study. The dimensions of the converter are given in Table 1.

2.1. Mathematical formulation

The axi-symmetric forms of the turbulent Reynolds averaged Navier–Stokes equations are discretized by a finite volume technique. The solution is obtained by using the FINE™ integrated CFD package of NUMECA International. Details of the solution procedure can be found in *FINE*™ theory documentation [10].

The existence of the monolith is simulated by a porous medium with a prescribed pressure drop. The flow through the monolith is treated as laminar and the pressure drop per unit length is calculated by using the Hagen–Poiseuille equation defined as

$$\frac{\Delta p}{L} = \frac{28.5}{d_h^2}\mu u \quad \text{in [Pa/m]}, \tag{1}$$

Table 1
Geometrical data of the catalytic converter

Parameter	Value	Units
Monolith diameter	100	mm
Monolith length	100 (long)	mm
	50 (short)	
Channel density	62	channels/cm^2
	400	channels/in^2
Substrate wall thickness	0.17	mm
Channel hydraulic diameter	1	mm
Open frontal area	75	%
Inlet diffuser length	25	mm
Outlet cone length	25	mm
Inlet pipe inner diameter	47	mm
Outlet pipe inner diameter	47	mm

where μ is the dynamic viscosity which is a function of the temperature, u is the velocity through the effective area of the porous medium in the x-direction and d_h is the hydraulic diameter of each single passage that form the monolith. The pressure drop term is treated as an additional source term in the solution procedure of the discretized equations.

The flow upstream and downstream the monolith is treated as turbulent and the low Reynolds version of the k–ε model [11] is used for the turbulence modelling. In addition, the Reynolds stresses are expanded up to the quadratic terms (beyond to the Boussinesq's linear approximation) and thus a non-linear eddy viscosity model is adopted by modifying accordingly the production term of the turbulence kinetic energy. Details for the turbulence modelling can be found also in [10].

2.2. Boundary conditions

2.2.1. Inlet

The mass flow rate and the flow temperature at the inlet of the computational domain are prescribed. The inlet was located 20 diameters upstream from the beginning of the diffuser, and plug flow velocity distribution was assumed. For the turbulence quantities, the turbulence kinetic energy is computed by using the equation

$$k = 1.5(Tu \cdot u_{\mathrm{ref}})^2, \tag{2}$$

where u_{ref} is the mean velocity corresponding at the selected mass flow rate through the inlet area and Tu is the turbulence level. For the last, the lack of experimental data led to the use of a value equal to 5%, which is a typical value for internal channel flows. The value of the turbulence dissipation rate ε is calculated using the semi-empirical equation:

$$\varepsilon = \frac{c_\mu}{50}\rho_{\mathrm{ref}}\frac{k^2}{\mu_{\mathrm{ref}}}, \tag{3}$$

where $c = 0.09$, ρ_{ref} and μ_{ref} are the fluid's density and dynamic viscosity at the inlet and k is the turbulence kinetic energy.

2.2.2. Outlet

The pressure at outlet (which is located about twenty pipe diameters downstream the monolith) is set equal to the ambient pressure and the mass flow rate through the exit section is corrected at each iteration in relation with the mass flow rate at inlet.

2.2.3. Solid walls

The walls are treated as adiabatic. Special care is taken to the location of the computational nodes near the wall. Since the low Reynolds variant of the k-ε model is used, the computational mesh is constructed to have the dimensionless local normal distance from the wall, y^+, less than 1 for at least five nodes.

2.3. Computational grid and solution procedure

A structured grid having 32 930 computational nodes is used for the simulation of the computational domain. This size was found to give grid-independent solutions for all the test cases examined in this work. Fig. 2. shows the computational domain and a detailed view of the grid used in the region near the intersections of the inlet pipe with the diffuser and of the diffuser with the porous medium simulating the monolith. The area occupied by the insulating material, as shown in Fig. 1, was accounted for in the formulation of the grid near the diffuser—monolith interface.

The geometry of the monolith is simulated with an individual cylindrical block (shown between the diffuser and the nozzle of the computational configuration), which imposes to the fluid flow the prescribed pressure drop.

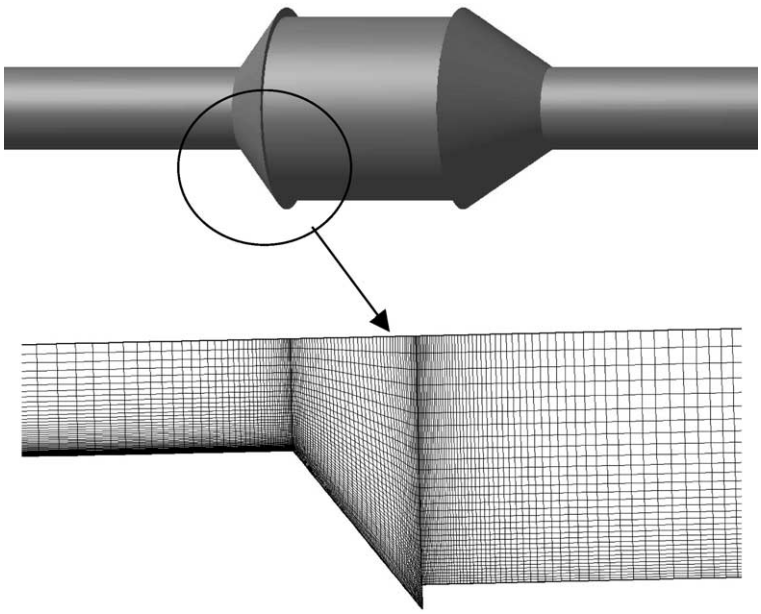

Fig. 2. The computational domain and a detailed view of the grid used inside the channel. Inlet is located at left.

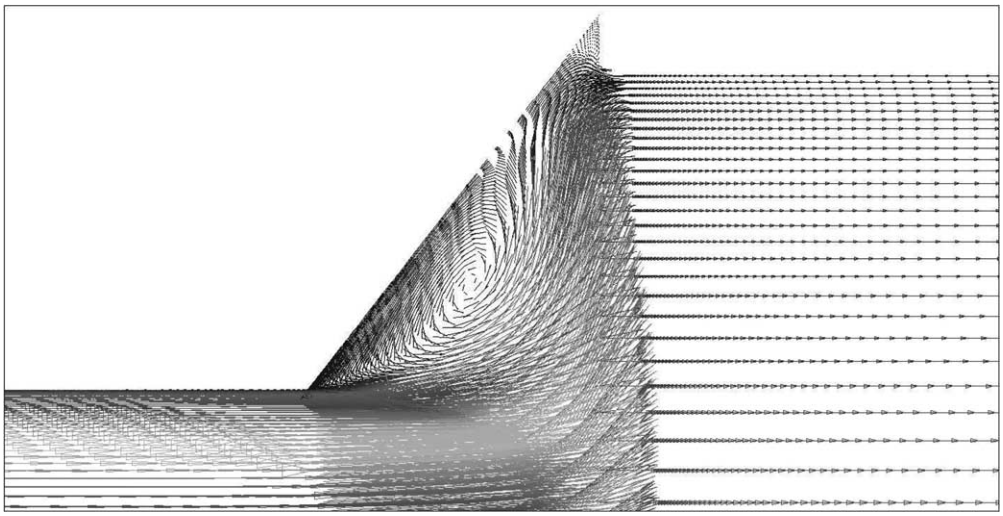

Fig. 3. Vector plot in the diffuser walls upstream the monolith's inlet section.

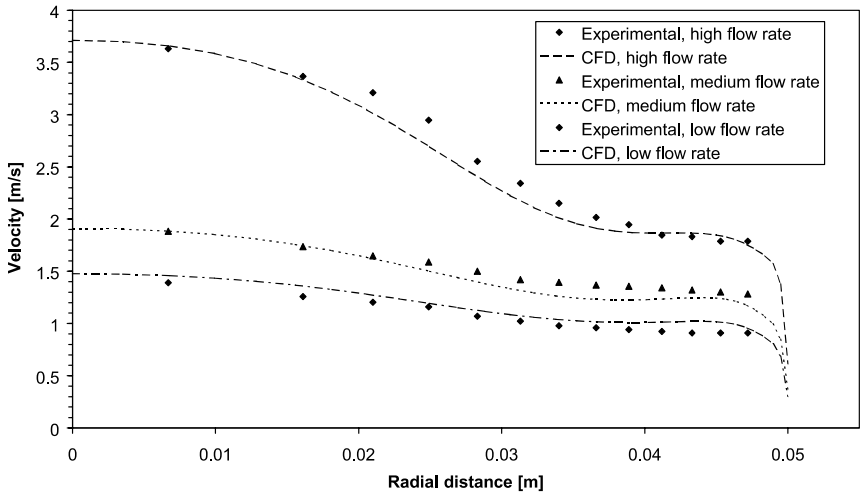

Fig. 4. Comparisons CFD—experimental data. Exhaust gas temperature: 300 K, monolith length: 100 mm.

The iterative solution procedure is performed by using the multigrid technique, in order to accelerate the convergence. Two coarser grids are used and after a certain number of preliminary iterations the solver switches to the solution procedure in the fine grid. Convergence is reached when the averaged residuals for the solved quantities, i.e. velocity components, turbulence quantities and mass balance are less than 10^{-4}. The average CPU time to achieve convergence for each case was found to be about 6 h in an Intel Pentium™ 1.0 GHz PC.

2.4. Computational results

The velocity vector field in the axi-symmetric plane of the intersection between the diffuser and the monolith for a mass flow rate corresponding to 0.021 kg/s is shown in Fig. 3. There is a large separation region in the diffuser's walls, which strongly affects the radial distribution of the longitudinal velocity at monolith inlet phase.

Previously published experimental results [12] are used to validate the CFD simulation results. Validation is performed by comparing the gas velocity profiles at the monolith outlet, as calculated by the CFD software, against the ones obtained experimentally, for the previously described converter setup. Fig. 4 presents the respective comparison for three different exhaust gas flow rates, at 300 K. A good agreement is obtained in all three cases, which highlights the accuracy of the employed CFD technique.

3. Flow resistance modelling

In this section, a simplified modelling approach to calculate the flow distribution at the inlet face of catalytic converter monoliths with axi-symmetric geometries will be presented. This semi-empirical approach is based on the simulation of the 2-D flow phenomena in the inlet and outlet cones by 1-D flow passages that induce equivalent flow resistance (flow resistance modelling).

3.1. Model formulation

The geometry, including the inlet cone, the catalyst monolith and the outlet cone is divided in axial and radial nodes as shown in Fig. 5. The first axial node corresponds to the inner cone and the last axial node to the outer cone. The inlet of the first axial node is located one diameter upstream from the diffuser inlet. At that plane, CFD simulation results show that the pressure

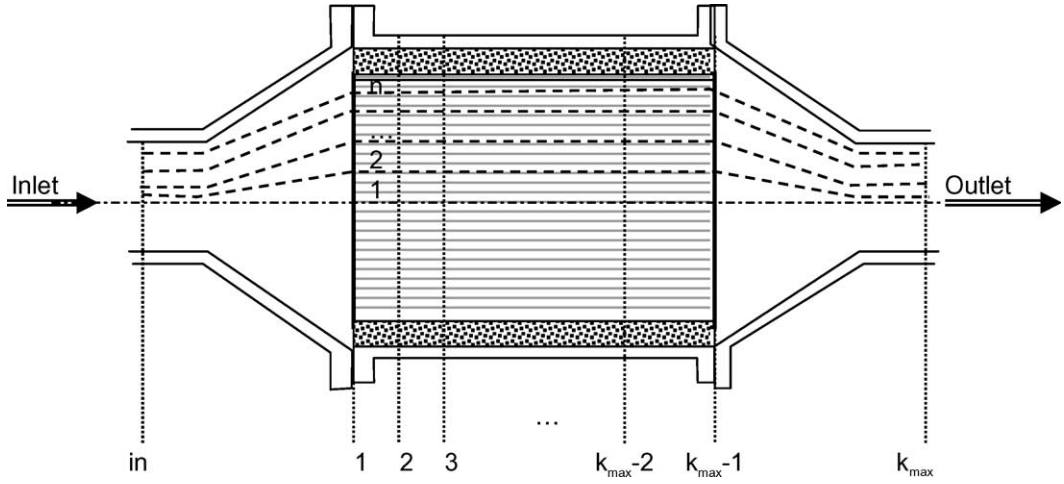

Fig. 5. Axial and radial node arrangement, used in the flow resistance model.

distribution is uniform (radial pressure variations are less than 2 Pa). Similarly, the outlet plane of the last node is located one diameter downstream from the end of the outlet cone, where the pressure distribution can be considered uniform. The radial nodes are distributed so as to form n concentric ring-form sections of equal cross-area at each axial node.

With the pressure at the exit of the outlet cone and the total mass flow rate given, the problem is to compute the distribution of the mass flow as a function of radial distance at the inlet face of the catalyst monolith. The computation of the flow distribution is based on an iterative procedure, consisting of the following steps.

Step 1. Assumption of initial arbitrary values for total pressure drop between inlet and outlet cones Δp_{tot}. Assuming initially equal values of $\dot{m}_i$ and satisfying the mass balance $\dot{m} = \sum_{i=1}^{n} \dot{m}_i$, we have

$$\dot{m}_i = \frac{\dot{m}}{n}, \quad i = 1, \ldots, n. \tag{4}$$

Step 2. As discussed in the previous section, the flow in the inlet cone section is usually characterized by separation phenomena, which induce additional pressure losses rendering the flow conditions far from being ideal. Typically this results in preferential flow localization near the symmetry axis in contrast with the periphery region.

In this simplified model, it is considered that the flow elements in each radial node in the inlet cone are subjected to 1-D friction losses as they travel to the monolith inlet face. These friction losses should be equivalent to the losses induced by the 2-D phenomena encountered in the inlet cone (wall friction, flow separation effects, oblique flow etc). To describe the pressure losses, one can rely on the usual approach for the calculation of pressure losses in conical diffusers [13]. The pressure drop formula in our case applies individually for all radial nodes as below

$$\Delta p_{i,1} = p_{\text{in}} - p_{i,1} = \frac{\dot{m}_i^2}{2\rho A_{i,\text{in}}^2}\left[\left(1 - \frac{A_{i,\text{in}}^2}{A_i^2}\right) + \zeta_i\left(1 - \frac{A_{i,\text{in}}}{A_i}\right)^2\right]. \tag{5}$$

In the above formula the parameter ζ_i represents a pressure loss coefficient. For ideal, frictionless flow $\zeta_i = 0$, for every node, and Eq. (5) is equivalent to the Bernoulli law. To simulate a real diffuser, one has to determine the values of ζ_i for each node, based in principle on experimental data. This procedure will be discussed in the next chapter.

With the inlet pressure and flow rates given, the pressure field can be computed stepwise along the catalyst monolith for each node (i, k) with suitable pressure drop relations. The flow in the monolith channels is always laminar for the operating conditions in automobile exhaust. The pressure drop formula may be written

$$\Delta p_{\text{lam},i,k\to k+1} = p_{i,k} - p_{i,k+1} = \frac{28.5\mu u_{ik}}{d_{h,ik}^2}\Delta x, \tag{6}$$

with

$$u_{ik} = \frac{\dot{m}_i}{\rho A_{ik}\text{vfr}_{ik}}. \tag{7}$$

In the outlet cone section, separation is not expected and the flow may be considered frictionless and ideal. The pressure difference is computed by the Bernoulli law

$$\Delta p_{i,k\max-1\to k\max} = p_{i,k\max-1} - p_{i,k\max} = \frac{\dot{m}_i^2}{2\rho A_{i,k\max-1}^2}\left(1 - \frac{A_{i,k\max-1}^2}{A_{i,k\max}^2}\right). \tag{8}$$

Based on the pressure drop relations, we can compute stepwise the pressure along the monoliths and thus the pressure at the final axial node for each ring section, $p_{i,k\ \max}$. The resulting computed pressure loss for each ring section is

$$\Delta p_i = p_{\text{in}} - p_{i,k\max}. \tag{9}$$

Step 3. If the computed pressure losses Δp_i for all ring sections are numerically equal to Δp_{tot} the flow and pressure field has been solved. In the opposite case, the assumed values for total pressure loss and flow rates should be corrected, according to step 4.

Step 4. The following corrections for the flow distribution and total pressure loss are applied:

$$\Delta p'_{\text{tot}} = \frac{\dot{m}}{\sum_{i=1}^{n} \frac{\dot{m}_i}{\Delta p_i}}, \tag{10}$$

$$\dot{m}'_i = \frac{\Delta p'_{\text{tot}}}{\Delta p_i}\dot{m}_i. \tag{11}$$

It may be easily shown that the above equations satisfy the mass balance $\dot{m} = \sum_{i=1}^{n} \dot{m}'_i$.

We then repeat the computation procedure starting from Step 2. The iterative algorithm converges quickly. For transient simulations, the computed values for total backpressure and individual flow rates are provided as input for the next time step, to minimize the required iterations. The CPU time required for a catalyst setup as the one shown in Fig. 5, with 14 radial and 20 axial nodes is in the order of milliseconds with an Intel Pentium™ 1 GHz processor.

3.2. Flow resistance model validation

In order to validate the accuracy of the proposed methodology, the obtained velocity profiles at the catalyst inlet face are compared with respective velocity profiles calculated using CFD. The individual flow resistance factors ζ_i for each radial node, are semi-empirical coefficients, which have to be calculated by a fitting procedure, in order to obtain good agreement between the results of the flow resistance and CFD model. The following procedure is followed to reduce the number of tunable parameters. Firstly, the gas velocity u_i corresponding to each radial node, is calculated using CFD. Based on these data, the value of each ζ_i is calculated by the formula

$$\zeta_i = \zeta_{\max}\left(\frac{u_{\max} - u_i}{u_{\max} - u_{\min}}\right)^2, \tag{12}$$

which is based on the second-order pressure loss dependence on flow velocity. The maximum flow resistance factor $\zeta_{\max}$, corresponding to the outer radial node, is now the only "tunable" parameter, which defines the degree of flow uniformity at the monolith inlet. Its value is selected using a try-and-error approach, until a good fit is achieved between the velocity profiles calculated by CFD and those calculated using the flow resistance model (FRM).

This process is performed using the velocity profile calculated by the CFD software for the previously described catalyst setup, with a mass flow rate of 0.021 kg/s at 300 K. Afterwards, the simulation is repeated for three different exhaust gas mass flow rates (0.021, 0.0125 and 0.01007 kg/s). The potential of the FRM methodology to simulate flow distribution at different temperatures, is examined by performing the same set of simulations at three different temperatures, namely 300, 750 and 1200 K. A total of nine cases are therefore simulated, using the same flow resistance factors. The results are presented in Figs. 6–8. A good fitting is achieved between CFD results and results obtained by the simplified FRM. In order to further examine the applicability of FRM the same set of simulations is performed with a 50 mm long monolith (half in length than the original configuration). The results for the 750 K test case are presented in Fig. 9. Again, a good agreement is observed between CFD and FRM results. Comparing this set of results with the ones obtained for the long monolith at the same temperature (Fig. 7) we can observe that the velocity profile in the case of the long monolith is more uniform. This is attributed to the fact that the long monolith imposes a higher pressure drop, which tends to "dampen" the diffuser effects on flow distribution. Interestingly, the FRM approach is able to predict the effect of different monolith lengths quite accurately. These results suggest that a single set of flow resistance factors ζ_i is able to characterize the effect of diffuser on flow distribution in a wide range of operating conditions.

The flow maldistribution can be quantified by using γ (gamma factor), an index of flow uniformity [5]. γ is defined as

$$\gamma = 1 - \frac{\omega}{2}, \tag{13}$$

where ω is an index of non-uniformity of the flow, defined as

$$\omega = \frac{\sum \omega_i}{n} \tag{14}$$

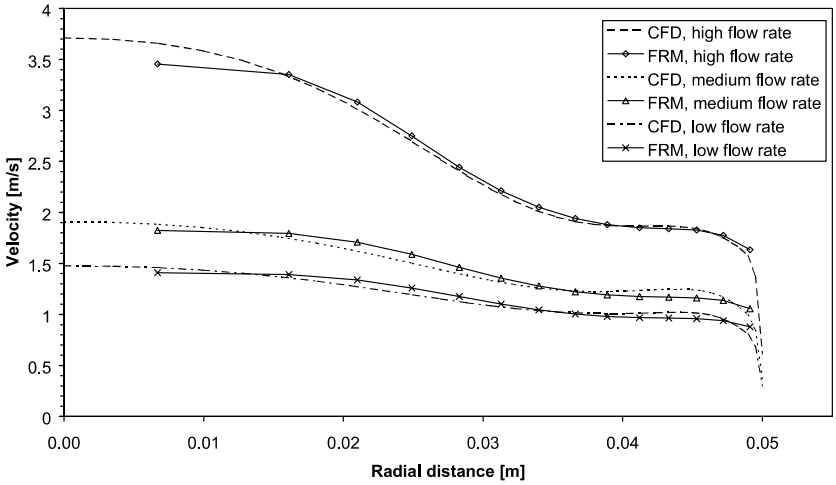

Fig. 6. Comparisons CFD—FRM. Exhaust gas temperature: 300 K, monolith length: 100 mm.

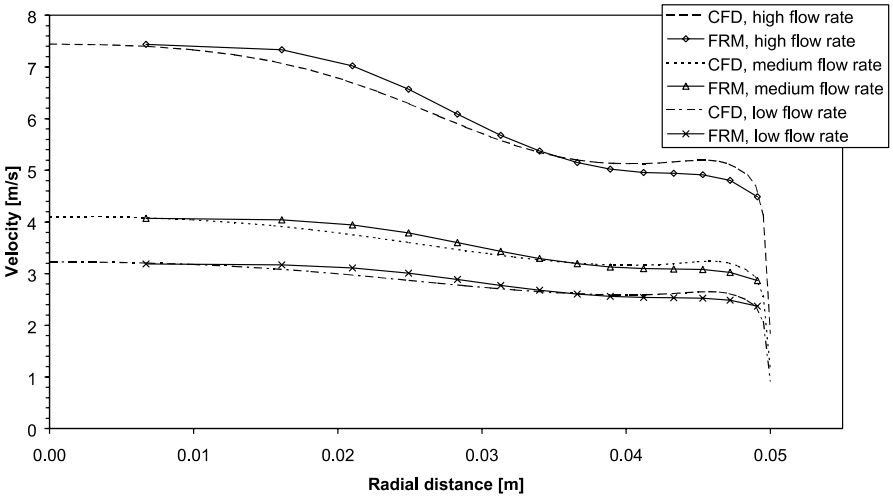

Fig. 7. Comparisons CFD—FRM. Exhaust gas temperature: 750 K, monolith length: 100 mm.

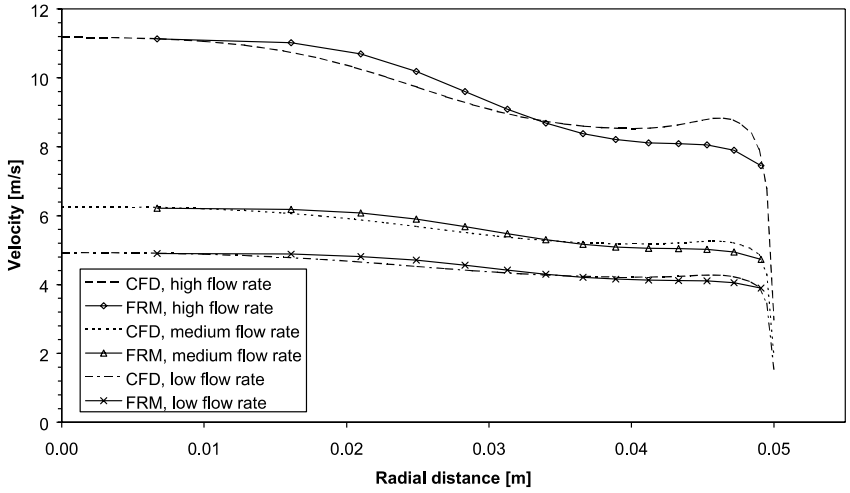

Fig. 8. Comparisons CFD—FRM. Exhaust gas temperature: 1200 K, monolith length: 100 mm.

with

$$\omega_i = \frac{|u_i - \bar{u}|}{\bar{u}}. \tag{15}$$

By definition, $\gamma = 1$ corresponds to uniform flow. Table 2 summarizes the calculated values of the gamma factor, based on the velocity profiles returned by the two modelling methods. A noticeable discrepancy between CFD and FRM gamma factor is observed only in the case of the short monolith and high mass flow rate at 300 K. Although it would be possible to overcome this discrepancy by manually "tuning" each flow resistance factor for this specific case, this is not

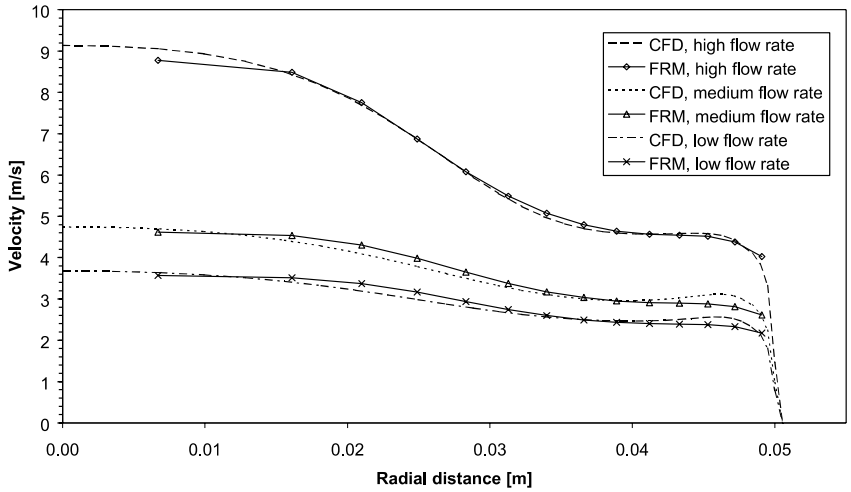

Fig. 9. Comparisons CFD—FRM. Exhaust gas temperature: 750 K, monolith length: 50 mm.

Table 2
Pressure drop and gamma factor values obtained by CFD and FRM

Temperature [K]	Mass flow [kg/s]	Pressure drop [Pa]		Gamma factor	
		FRM	CFD	FRM	CFD
(a) For the long monolith (100 mm length)					
300	0.01007	82.1	81.9	0.9307	0.9247
300	0.0125	106.3	104.5	0.9192	0.9141
300	0.021	201.6	204.4	0.8872	0.8651
750	0.01007	346.9	344.6	0.9566	0.9581
750	0.0125	443.1	440.3	0.9487	0.9511
750	0.021	809.9	812.9	0.9253	0.9277
1200	0.01007	735.5	705.4	0.9667	0.9683
1200	0.0125	932.3	894.5	0.9603	0.9625
1200	0.021	1674.5	1668.7	0.9410	0.9494
(b) For the short monolith (50 mm length)					
300	0.01007	47.8	48.7	0.8898	0.8653
300	0.0125	63.0	65.7	0.8749	0.8377
300	0.021	124.0	136.6	0.8361	0.7571
750	0.01007	193.6	190.4	0.9271	0.9189
750	0.0125	251.0	246.8	0.9153	0.9067
750	0.021	477.7	487.3	0.8826	0.8569
1200	0.01007	402.5	382.4	0.9422	0.9331
1200	0.0125	518.1	492.5	0.9325	0.9217
1200	0.021	964.8	929.9	0.9040	0.8921

done, as it would sacrifice the simplicity of the proposed methodology. In all other cases, the relatively good match between CFD and FRM results verify the good fit observed visually in the velocity profiles in Figs. 6, 7, and 9.

In the same table, pressure drop values across the catalytic converter, i.e. inlet cone, monolith and outlet cone, as calculated by CFD and FRM are also displayed. Pressure drop is an important issue in the design of catalytic converters, as it affects strongly the engine performance. Table 2 shows that the pressure drop calculated by the FRM methodology presents a good agreement with the one predicted by the commonly applied CFD method, which can be considered accurate for this type of calculations. The deviation between CFD and FRM results generally lies between 0.5% and 5%. Again, the only important discrepancy is found in the case of the short monolith and high mass flow rate, at 300 K. Fig. 10 visualizes the above results, plotting the CFD- and FRM-predicted pressure drop as a function of exhaust gas temperature and mass flow rate.

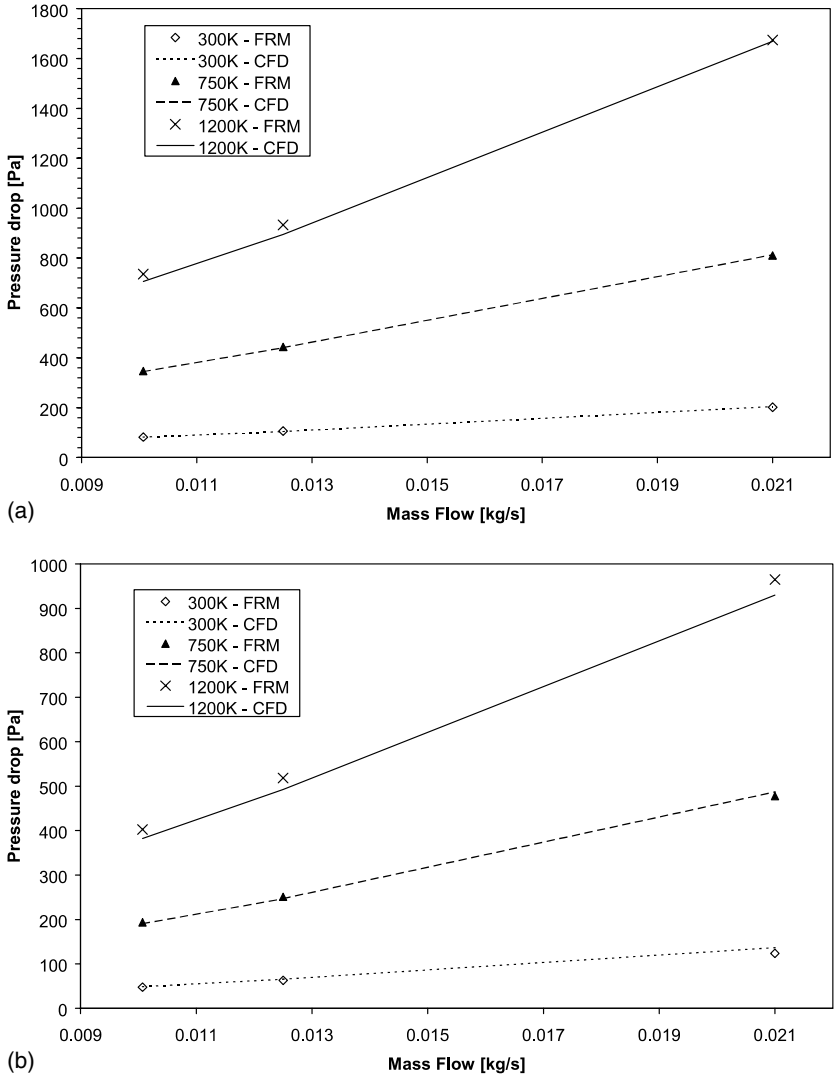

Fig. 10. Pressure drop at the catalytic converter as a function of exhaust gas temperature and mass flow rate: (a) long monolith (100 mm) and (b) short monolith (50 mm).

The results presented in this chapter indicate that, once the flow resistance factors ζ_i are determined based on Eq. (12), they can be applied to simulate the flow distribution at the monolith inlet, for a wide range of gas temperature and mass flow rate. The advantage of employing the FRM technique is more obvious in the case of transient simulations, typically requiring more than 1000 time steps to simulate the warming up and light-off performance of a catalytic converter. This is discussed in more detail in the next chapter.

4. Coupling with transient heat transfer

The coupling of the CPU-efficient Flow Resistance Modelling with transient models for the computation of heat response in catalyst monoliths is the subject of the present section. For illustration purposes, we will confine our interest in the warm-up operation of the catalyst during cold start. For reasons of simplicity, it can be assumed that during this warm-up period, the oxidation reaction rates of CO and hydrocarbons are practically insignificant and the associated exothermy may be neglected. Axial and radial temperature gradients inside the catalyst monolith may occur due to ambient heat losses and inlet flow non-uniformities.

The basic heat transfer mode is convection between exhaust gas and solid phase in the channels of the monolithic substrates [14]. The Nu number for the laminar flow in the channels approximates the solution of the Graetz–Nusselt problem for constant wall temperature. The methodology employed to deposit the active washcoat in the initially square monolith channels results in a circular channel geometry. For laminar flow in circular channels with the introduction of a correction for entrance effects we have

$$Nu = 3.66\left(1 + \frac{0.095}{x^*}\right)^{0.45}. \tag{16}$$

The 2-D axi-symmetric grid described above is used to model the heat transfer. Each radial ring-section contains a large number of internal channels. With a given temperature and velocity distribution at the monolith inlet, representative inlet conditions can be defined for all channels contained in each monolith radial section.

The transient thermal response of each monolith is computed as a series of quasi steady-states [15]. Thus, the solution procedure followed in each time marching comprises the following steps:

- Computation of the convective heat transfer from the exhaust gas to the monolith surface for each ring section.
- Computation of the 2-D transient temperature field in the cylindrical converter, taking into account the heat conduction in the monolith. The contribution of the convective heat transfer in the channels (computed in the previous step) is taken into account by respective source terms.

The first step involves the computation of the gas temperature for each node $(i, k+1)$ given the conditions in the node (i, k). Employing locally analytical solutions [16,14] with the dimensionless length ξ defined in Nomenclature, we obtain

$$T_{g,k+1} = T_{s,k} + (T_{g,k} - T_{s,k})\mathrm{e}^{-\Delta\xi}. \tag{17}$$

After the determination of the temperature distribution along the channel, the corresponding convective heat rates on a volume basis may be computed for each space step according to the following balance equation:

$$\dot{q}_{\mathrm{conv},ik} = \frac{\dot{m}_i \cdot C_{p,\mathrm{g}}}{A_i \Delta\xi} \cdot (T_{\mathrm{g},ik+1} - T_{\mathrm{g},ik}). \tag{18}$$

In the next computational step, the temperature field in the converter is described by the transient heat conduction equation with heat sources in cylindrical co-ordinates

$$\rho_{\mathrm{s}} C_{p,\mathrm{s}} \frac{\partial T_{\mathrm{s}}}{\partial t} = \lambda_{\mathrm{s},x} \frac{\partial^2 T_{\mathrm{s}}}{\partial x^2} + \lambda_{\mathrm{s},r} \frac{1}{r} \frac{\partial}{\partial r}\left(r \frac{\partial T_{\mathrm{s}}}{\partial r} \right) + \dot{q}_{\mathrm{conv}}. \tag{19}$$

The values of ρ_{s}, $C_{p,\mathrm{s}}$, $\lambda_{\mathrm{s},x}$, $\lambda_{\mathrm{s},r}$ depend on the respective grid node. For the nodes included in the monoliths, bulk values are computed for the above parameters, according to the respective void fraction. For the nodes of the surrounding insulation, the corresponding properties are used.

The boundary conditions for the heat conduction equation at the outer radius taking into account heat convection and radiation to ambient will be

$$\lambda_r \left.\frac{\partial T}{\partial r}\right|_{r=r_{\mathrm{out}}} = h_{\mathrm{amb}}(T - T_{\mathrm{amb}}) + \varepsilon \cdot \sigma \cdot (T^4 - T_{\mathrm{amb}}^4) A. \tag{20}$$

From the symmetry condition at $r = 0$

$$\left.\frac{\partial T}{\partial r}\right|_{r=0} = 0. \tag{21}$$

In the axial direction, heat transfer from the monolith edges is negligible. The respective boundary conditions for each monolith are:

$$\left.\frac{\partial T}{\partial x}\right|_{x=x,\mathrm{first}} = 0 \quad \text{and} \quad \left.\frac{\partial T}{\partial x}\right|_{x=x,\mathrm{last}} = 0. \tag{22, 23}$$

The 2-D transient temperature field in each monolith is solved using the "Alternate Direction Implicit" (ADI) technique, which offers stability advantages with moderate computation effort.

Starting from an initial condition for the temperature field in the monolith, the flow resistance model can be applied to compute the initial flow field. The above described transient 2-D thermal response model is used to compute the temperature field for the next time step. In the next time step the "flow resistance" calculations are repeated taking into account the new boundary conditions at catalyst inlet (gas flow rate, temperature). Even if the inlet gas conditions remain constant, the flow field may change with time, as a result of the change in the temperature field of the catalyst monolith. The latter affects significantly the exhaust gas properties involved in the solution of the flow resistance model.

5. Transient model application

This section presents a typical example of the coupling of FRM, described in Chapter 3 with a transient 2-D heat transfer model, described in Chapter 4. The test case examined, is the warm-up

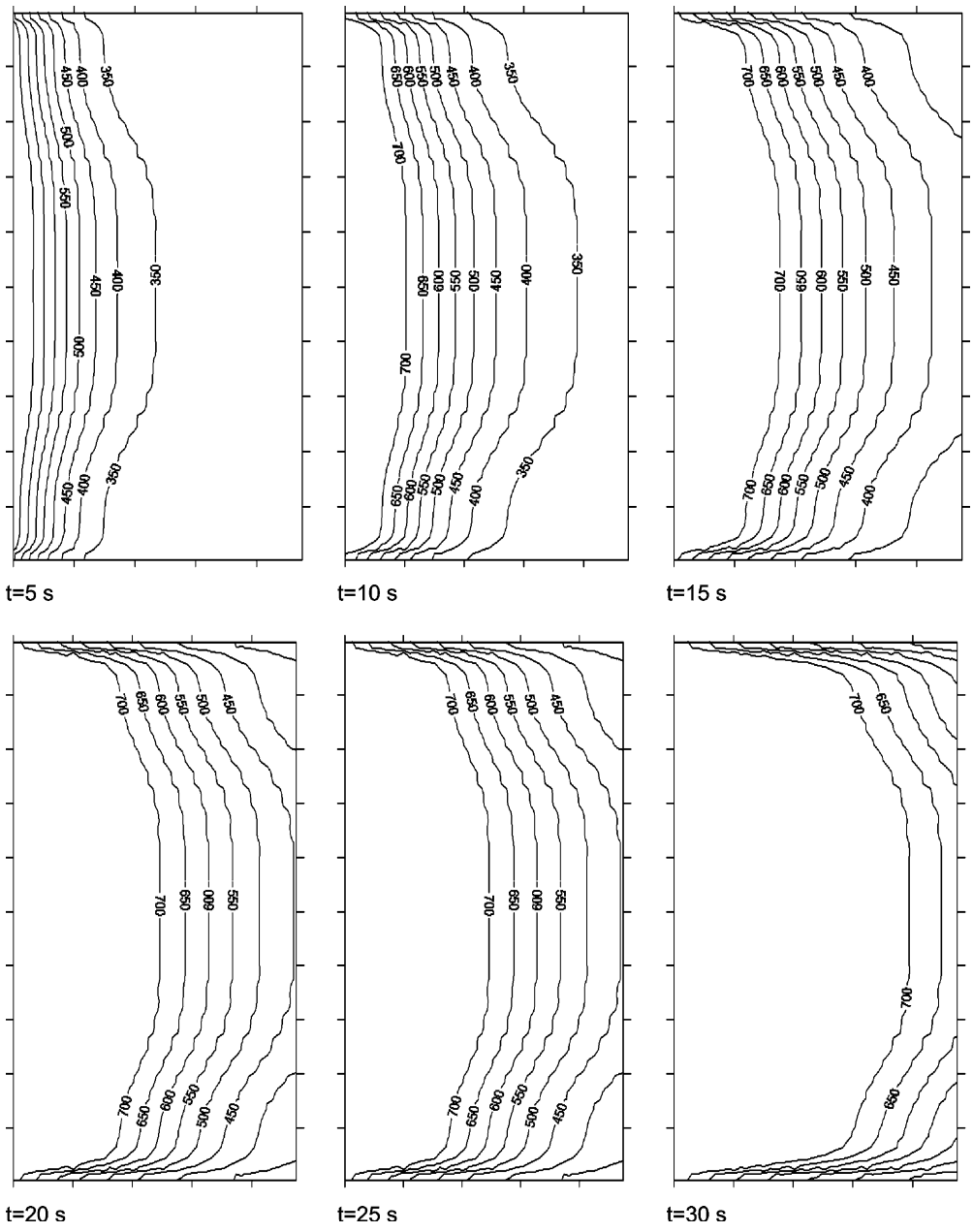

Fig. 11. Transient 2-D temperature profiles inside the monolith during the light-off phase.

behavior of a close-coupled catalytic converter. For simplicity reasons, the heat released or consumed by chemical reactions is not taken into account.

At the beginning of the light-off test, the temperature of the catalytic converter is equal to ambient (300 K). The catalytic converter (50 mm length and 100 mm diameter) is exposed to

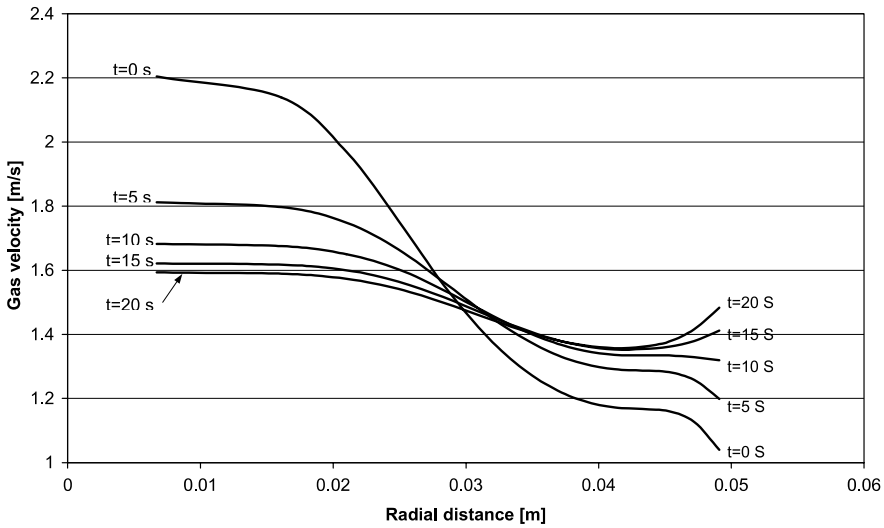

Fig. 12. Velocity profiles at monolith inlet during the light-off phase.

exhaust stream of constant temperature (800 K) and mass flow rate (0.005 kg/s). These conditions are considered representative for close-coupled catalyst warm-up when the engine operates at idle mode.

The computation of the catalyst thermal response is a function of the radial flow distribution at the inlet face. In turn, the flow distribution is affected by catalyst the temperature field, since the pressure loss is a function of the local temperature (Eqs. (4)–(11)). Fig. 11 presents the 2-D temperature profiles inside the monolith as a function of time, during the warm-up phase. Fifteen seconds after engine start, the front part of the monolith (approximately 12 mm from the inlet face) has already reached temperatures higher than 700 K, which ensures that pollutant conversion would have already begun at that time. Such temperature profiles are very useful, mostly for assessing different substrate materials and formulations.

As the temperature inside the monolith rises, the velocity profile changes. Fig. 12 depicts this change. We observe a severe maldistribution when the converter is still cold, and the velocity profile gradually becomes more uniform, as the converter warms up. After 15–20 s from the engine start, the change in the flow distribution tends to become insignificant.

The computational time required for performing such a warm-up test is less than a minute with an Intel Pentium™ computer operating at 1 GHz, i.e., approximately two times longer than the duration of the simulated test. This computational time is many orders of magnitude lower than previously published transient CFD results [8], where a warm-up test consisting of 1000 time steps, takes 526.4 CPU hours on a SGI Indigo 2 processor.

6. Conclusions

The transient catalytic converter performance is governed by complex interactions between exhaust gas flow and the monolithic structure of the catalytic converter. During typical operating

conditions of interest (e.g. catalyst warm-up), one has to take into account the effect of the inlet diffuser on the flow field at the entrance and the resulting interactions with catalyst transient thermal response. CFD is a powerful tool for predicting the flow field at the inlet and outlet cones of catalytic converters, and has therefore been widely used in previous research works. However, its applicability is usually limited to steady-state simulations, due to the high computational times involved in transient CFD simulations. A novel simplified approach towards the solution of this problem in a rational and time efficient way was presented in this paper. A simplified methodology to predict the flow field at the inlet face of axi-symmetric catalytic converters was presented and validated against results of CFD simulations for a wide range of temperature and mass flow conditions. The CFD simulations in turn, were compared with respective experimental data published in the literature. The advantages of the flow resistance modelling approach can be summarized as:

- Mathematical simplicity, therefore minimum CPU requirements.
- The tunable parameters depend only on the converter geometry and not on the operating conditions and can be defined based on velocity profiles obtained experimentally or by CFD simulations. A correlation between the flow resistance factors can be obtained, thus reducing the number of tunable parameters down to one for the simplest axi-symmetric geometries. For more complex geometry a manual fine tuning of each flow resistance factor is necessary.
- Straightforward coupling with existing models for transient catalytic converter modelling.

In conclusion, in the present work, flow resistance model is developed and applied for the case of cylindrical monoliths, allowing an axi-symmetric approach. Extending the model to non-cylindrical 3-D geometries is in principle possible. This could probably be a subject of future work.

References

[1] G.C. Koltsakis, A.M. Stamatelos, Catalytic automotive exhaust aftertreatment, Progr. Energy Combust. Sci. 23 (1997) 1–39.
[2] A.P. Martin, N.S. Will, A. Bordet, et al., Effect of flow distribution on emissions performance of catalytic converters, SAE Paper 980936, 1998.
[3] D.W. Wendland, W.R. Matthes, Visualization of automotive catalytic converter internal flows, SAE Paper 861554, 1986.
[4] M.C. Lai, T. Lee, J.Y. Kim, et al., Numerical and experimental characterizations of automotive catalytic converter internal flows, J. Fluids Struct. 6 (1992) 451–470.
[5] H. Weltens, H. Bressler, F. Terres, et al., Optimisation of catalytic converter gas flow distribution by CFD prediction, SAE Paper 930780, 1993.
[6] W. Taylor III, CFD prediction and experimental validation of high-temperature thermal behavior in catalytic converters, SAE Paper 1999-01-0454, 1999.
[7] S. Sugiura, K. Ijuin, T. Yamada, et al., A multi-dimensional numerical method for predicting warm-up characteristic of automobile catalytic converter systems, SAE Paper 952413, 1995.
[8] S.-J. Jeong, W.-S. Kim, Three-dimensional numerical study on the use of warm-up catalyst to improve light-off performance, SAE Paper 2000-01-0207, 2000.
[9] M.E. Berkman, A. Katari, Transient CFD: how valuable is it for catalyst design? SAE Paper 2002-01-0064, 2002.

[10] FINE™ Numeca's Flow Integrated Environment, User Manual, Version 5.2, June 2001.
[11] Z. Yang, T.H. Shih, New time scale based k-model for near-wall turbulence, AIAA J. 31 (7) (1993).
[12] N.S. Will, C.J. Bennett, Flow maldistributions in automotive converter canisters and their effect on emission control, SAE Paper 922339, 1992.
[13] WAERMEATLAS, VDI-Verlag GmbH, Duesseldorf, 1988.
[14] G.C. Koltsakis, Warm-up behavior of monolithic reactors under non-reacting conditions, Chem. Eng. Sci. 52 (17) (1997) 2891–2899.
[15] G.C. Koltsakis, P.A. Konstantinidis, A.M. Stamatelos, Development and application range of mathematical models for 3-way catalytic converters, Appl. Catal. B: Environ. 12 (1997) 161–191.
[16] J.R. Mondt, Adapting the heat and mass transfer analogy to model performance of automotive catalytic converters, J. Eng. Gas Turbines Power-Trans. ASME 109 (1987).